Metal-Site-Controlled Arene Coordination in a Heterobimetallic Bi–Rh Complex with Pyrene

ARTICLE *in* ORGANOMETALLICS · JULY 2008

Impact Factor: 4.13 · DOI: 10.1021/om8001763

Metal-Site-Controlled Arene Coordination in a Heterobimetallic Bi−Rh Complex with Pyrene

Evgeny V. Dikarev,* Bo Li, Andrey Yu. Rogachev, Haitao Zhang, and Marina A. Petrukhina*

Department of Chemistry, University at Albany, 1400 Washington Avenue, Albany, New York 12222

Received February 25, 2008

The reactivity of a heterobimetallic Bi−Rh trifluoroacetate paddlewheel complex toward an aromatic substrate has been tested in a solvent-free environment. As a result of the gas phase codeposition of $[BiRh(O_2CCF_3)_4]$ with pyrene, a novel organometallic product, $[BiRh(O_2CCF_3)_4 \cdot (C_{16}H_{10})]_\infty$, has been isolated in the single crystalline form. An X-ray diffraction study revealed an extended 1D polymeric structure with different metal−π-arene bonding at the Bi and Rh axial sites of the heterobimetallic core. Specifically, η^6-coordination of pyrene at the Bi end and η^2-coordination at the Rh end have been found crystallographically and then confirmed computationally. The title product thus provides a unique example of site-controlled arene coordination by a heterobimetallic Bi−Rh unit. DFT methods have been used to rationalize the bonding and to evaluate the energetics of metal−π-arene interactions at the opposite ends of $[BiRh(O_2CCF_3)_4]$. The results were compared with the corresponding data for homometallic analogues $[Rh_2(O_2CCF_3)_4 \cdot (C_{16}H_{10})]_\infty$ and $[Bi_2(O_2CCF_3)_4 \cdot (C_{16}H_{10})]_\infty$. The synthesis, structural, and DFT studies of the latter are reported here for the first time.

Introduction

Metal cation−π-arene interactions play a significant role in the chemistry of both main group and transition metals.[1] The importance of the former relates to the prominence of alkali metals in biological systems and their possible involvement in cation−π-interactions with arene functionalities of amino acids.[2] Among the heavier main group elements, interactions of silver cations with π-systems have been broadly studied and utilized in the design of various supramolecular networks.[3] The chemistry and reactivity of π-arene complexes of transition metals have been extensively investigated with applications in organic synthesis[4] and catalysis.[5]

The recent preparation of the first bismuth−rhodium carboxylates[6,7] has provided access to unique molecules that incorporate both main group and transition metal sites. The heterobimetallic core molecules, $[BiRh(O_2CR)_4]$, maintain a paddlewheel structure with a single bismuth−rhodium bond that is retained in solution and in the gas phase. They can be used as single-source precursors for multimetallic oxide materials as well as new, less-expensive rhodium(II) catalysts for organic synthesis. Importantly, the presence of two chemically different adjacent metal centers in $[BiRh(O_2CR)_4]$ opens up unique opportunities for metalloselective transformations that can be utilized in organic synthesis or catalysis. Interesting synergistic effects have already been seen when certain heterobimetallic catalysts show better performance than their homometallic counterparts.[8] This can result from one metal enhancing the reactivity of the other or, alternatively, from the two metals cooperating in chemical transformations by performing key reaction steps separately and sequentially, or simultaneously. In particular, a combination of hard and soft metal centers within the catalyst is well-documented to provide novel bimetallic cooperativity.[9] All these facts prompted us to look further into the coordination abilities of $[BiRh(O_2CR)_4]$.

Although different reactivity at the two open metal sites of $[BiRh(O_2CR)_4]$ was anticipated, an avid Lewis acidity toward O-donors previously had been seen at the rhodium site only, while the bismuth end showed neither Lewis acidic nor basic properties.[6,7] Since arenes are the only substrates that are known to coordinate in axial positions of both dirhodium(II,II) and dibismuth(II,II) tetratrifluoroacetate molecules, in this work we test the reactivity of the heterobimetallic Bi−Rh unit toward an aromatic ligand. The gas phase deposition of $[BiRh(O_2-$

* Corresponding authors. E-mail: dikarev@albany.edu; marina@albany.edu.

(1) (a) Schmidbaur, H. *Angew. Chem.* **1985**, *97*, 893–904. (b) Calderazzo, F.; Pampaloni, G. *J. Organomet. Chem.* **1995**, *500*, 47–60. (c) Bennett, M. A. *Coord. Chem. Rev.* **1997**, *166*, 225–254. (d) Deeming, A. J. *Metal Clusters in Chemistry*; Wiley-VCH: Weinheim, 1999; Vol. 1, pp 236−268. (e) Hubig, S. M.; Lindeman, S. V.; Kochi, J. K. *Coord. Chem. Rev.* **2000**, *200*, 831–873. (f) Ferdani, R.; Hu, J.; Leevy, W. M.; Pajewska, J.; Pajewski, R.; Villalobos, V.; Barbour, L. J.; Gokel, G. W. *J. Incl. Phenom. Macrocycl. Chem.* **2001**, *41*, 7–12. (g) Xue, Y.; Davis, A. V.; Balakrishnan, G.; Stasser, J. P.; Staehlin, B. M.; Focia, P.; Spiro, T. G.; Penner-Hahn, J. E.; O'Halloran, T. V. *Nat. Chem. Biol.* **2008**, *4*, 107–109.

(2) Gokel, G. W.; Barbour, L. J.; De Wall, S. L.; Meadows, E. S. *Coord. Chem. Rev.* **2001**, *222*, 127–154.

(3) (a) Munakata, M.; Wu, L. P.; Ning, G. L. *Coord. Chem. Rev.* **2000**, *198*, 171–203. (b) Kuroda-Sowa, T.; Liu, S. Q.; Yamazaki, Y.; Munakata, M.; Maekawa, M.; Suenaga, Y.; Konaka, H.; Nakagawa, H. *Inorg. Chem.* **2005**, *44*, 1686–1692.

(4) (a) Woodgate, P. D. *Adv. Detailed React. Mech.* **1995**, *4*, 93–127. (b) Kündig, E. P.; Pape, A. *Top. Organomet. Chem.* **2004**, *7*, 71–94.

(5) Rigby, J. H.; Kondratenko, M. A. *Top. Organomet. Chem.* **2004**, *7*, 181–204.

(6) Dikarev, E. V.; Gray, T. G.; Li, B. *Angew. Chem., Int. Ed.* **2005**, *44*, 1721–1724.

(7) Dikarev, E. V.; Li, B.; Zhang, H. *J. Am. Chem. Soc.* **2006**, *128*, 2814–2815.

(8) (a) Hermans, S.; Khimyak, T.; Raja, R.; Sankar, G.; Thomas, J. M.; Johnson, B. F. G. *Nanotechnol. Catal.* **2004**, *1*, 33–49. (b) Greeley, J.; Jaramillo, T. F.; Bonde, J.; Chorkendorff, I.; Nørskov, J. K. *Nat. Mater.* **2006**, *5*, 909–913. (c) Srivastava, R.; Mani, P.; Hahn, N.; Strasser, P. *Angew. Chem., Int. Ed.* **2007**, *46*, 1–5. (d) Li, X.; Iglesia, E. *Angew. Chem., Int. Ed.* **2007**, *46*, 8649–8652. (e) Messaoudi, A.; Deglmann, P.; Braunstein, P.; Hofmann, P. *Inorg. Chem.* **2007**, *46*, 7899–7909.

(9) Wheatly, N.; Klack, P. *Chem. Rev.* **1999**, *99*, 3379–3420.

10.1021/om8001763 CCC: $40.75
Publication on Web 07/11/2008

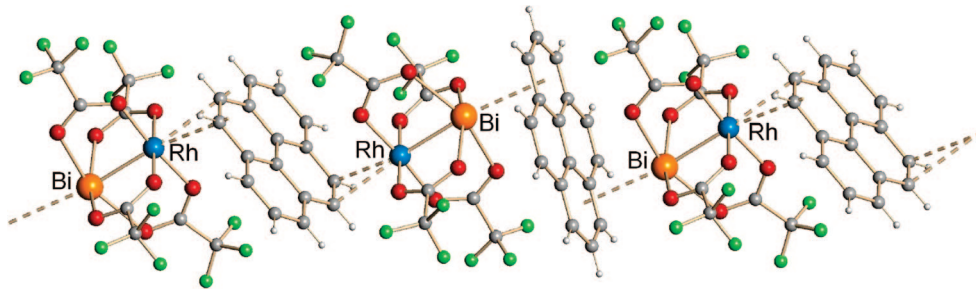

Figure 1. Fragment of the 1D chain in $[BiRh(O_2CCF_3)_4 \cdot (C_{16}H_{10})]_\infty$ (**1**). Bi···C 3.359(3), 3.400(3), 3.462(3), 3.530(3), 3.573(3), and 3.607(3) Å; Rh···C 2.681(3) and 2.708(3) Å.

$CCF_3)_4$] with pyrene ($C_{16}H_{10}$) under solventless conditions resulted in the isolation of a new crystalline organometallic product, $[BiRh(O_2CCF_3)_4 \cdot (C_{16}H_{10})]_\infty$. Its one-step synthesis and spectroscopic and structural characterization are reported here. This is followed by density functional theory calculations, which provide the first evaluation of how the presence of bismuth affects the coordination properties of rhodium in the paddle-wheel $[BiRh(O_2CCF_3)_4]$ molecule and vice versa. For comparison, the structural and computational studies of the corresponding homometallic complexes with pyrene are also presented.

Results and Discussion

Utilizing solvent-free reaction conditions that allow us to study intermolecular interactions without interfering solvent effects,[10] the heterobimetallic $[BiRh(O_2CCF_3)_4]$ complex has been cosublimed with pyrene in a sealed ampule at 100 °C. This reaction afforded red crystals of a new arene adduct, $[BiRh(O_2CCF_3)_4 \cdot (C_{16}H_{10})]$ (**1**), that were deposited in the cold end of the ampule in quantitative yield. Crystals of **1** display much better air and moisture stability than the parent bismuth−rhodium trifluoroacetate complex.[6] The IR spectrum of the crystalline product **1** shows a high-energy shift of about 13 cm^{-1} for C−H vibrations of the coordinated pyrene compared to the uncoordinated molecule. Interestingly, a similar shift for C−H stretching frequencies can be seen in a solution of **1** in CCl_4. The latter result indicates some degree of association between the heterobimetallic unit and pyrene in noncoordinating solvents, likely in the form of monoadducts. The ^1H NMR data for **1** in CD_2Cl_2 also reveal small but noticeable upfield shifts for the pyrene protons compared to the free ligand, in accord with the IR data.

The title compound **1** has also been characterized by elemental analysis and single-crystal X-ray diffraction. Its crystal structure is built of alternating heterobimetallic units and coordinated pyrene molecules that form a 1D organometallic polymer with a 1:1 composition of $[BiRh(O_2CCF_3)_4]$ to $C_{16}H_{10}$ (Figure 1).

Importantly, the coordination of pyrene is different at the two opposite ends of the heterobimetallic core. At the Rh end, the two shortest Rh···C_{arene} contacts are 2.681(3) and 2.708(3) Å, so that the pyrene ligand is acting in an η^2-mode toward rhodium(II). At the Bi end, pyrene has six Bi···C contacts that vary in the range from 3.359(3) to 3.607(3) Å and thus can be considered as η^6-coordinated. The Bi···$C_{centroid}$ distance of 3.19 Å can be compared with those of 3.05 and 3.23 Å in the 1D polymeric complexes of dibismuth(II,II) tetratrifluoroacetate with toluene[11] and hexamethylbenzene,[12] respectively.

Scheme 1. Clar Sextet Rule and Numbering for Pyrene

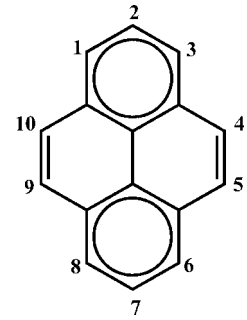

Another interesting structural feature of **1** is the alternation of orientations of the dimetal unit and pyrene along the chain (Figure 1). One pyrene η^6-coordinates to two bismuth centers from neighboring heterobimetallic units, while the other pyrene connects two different rhodium centers in an η^2-mode. Thus, the pyrene ligand functions either as an η^6:η^6-bridge toward bismuth or as an η^2:η^2-bridge toward rhodium with its different benzene rings being involved in coordination of Rh and Bi. This feature is best described by the Clar sextet rule (Scheme 1) that considers pyrene as comprised of two delocalized sextet rings and two fixed double bonds.[13] Due to intrinsic preferences of the above metals, Bi prefers to bind to the delocalized ring, while Rh coordinates to the localized carbon−carbon double bond of pyrene.

The Bi−Rh bond distance of 2.5766(3) Å in **1** is slightly elongated compared to that in the parent $[BiRh(O_2CCF_3)_4]$ complex (2.5493(3) Å). It is informative to compare the coordination of pyrene at the Rh end in **1** with that in the previously reported 1D polymer of dirhodium(II,II) tetratrifluoroacetate, $[Rh_2(O_2CCF_3)_4 \cdot (C_{16}H_{10})]_\infty$ (**2**).[14a] Thus, the Rh···C_{arene} interactions in **1** (averaged to 2.695 Å) are noticeably longer than those of 2.578 Å in the homometallic complex **2**. However, in both cases pyrene is acting as an $\eta^2(4,5)$:$\eta^2(9,10)$-bridge toward rhodium(II) centers. Such C−C bonds have the highest π-bond order and the shortest bond distance (1.321(7) Å) in the structure of free pyrene.[15] Thus, the electrophilic Rh(II)

(10) Petrukhina, M. A. *Coord. Chem. Rev.* **2007**, *251*, 1690–1698.
(11) Dikarev, E. V.; Li, B. *Inorg. Chem.* **2003**, *43*, 3461–3466.
(12) Frank, W.; Reiland, V.; Reiss, G. J. *Angew. Chem., Int. Ed.* **1998**, *37*, 2983–2985.
(13) Clar, E. *The Aromatic Sextet*; John Wiley and Sons Ltd.: London, 1972.
(14) (a) Cotton, F. A.; Dikarev, E. V.; Petrukhina, M. A. *J. Am. Chem. Soc.* **2001**, *123*, 11655–11663. (b) Petrukhina, M. A.; Andreini, K. W.; Mack, J.; Scott, L. T. *Angew. Chem., Int. Ed.* **2003**, *42*, 3375–3379. (c) Petrukhina, M. A.; Andreini, K. W.; Peng, L.; Scott, L. T. *Angew. Chem., Int. Ed.* **2004**, *43*, 5477–5481.
(15) (a) Hazell, A. C.; Larsen, F. K.; Lehmann, M. S. *Acta Crystallogr.* **1972**, *B28*, 2977–2984. (b) Kai, Y.; Hama, F.; Yasuoka, N. *Acta Crystallogr.* **1978**, *B34*, 1263–1270.
(16) Silvestru, C.; Breunig, H. J.; Althaus, H. *Chem. Rev.* **1999**, *99*, 3277–3327.

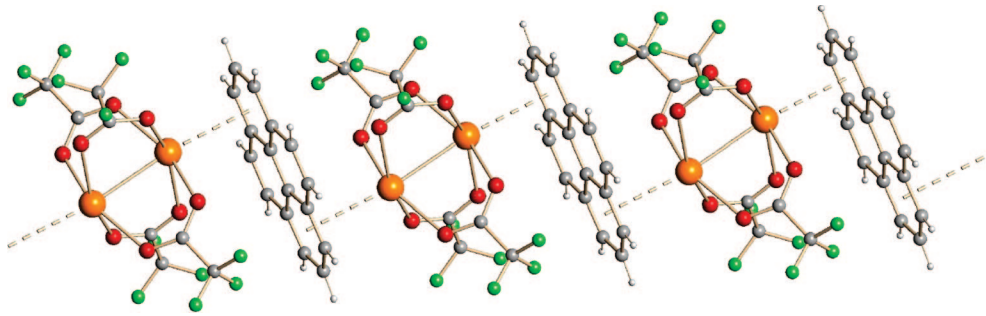

Figure 2. Fragment of the 1D chain in $[Bi_2(O_2CCF_3)_4 \cdot (C_{16}H_{10})]_\infty$ (**3**). Bi···C 3.432(4), 3.442(4), 3.473(5), 3.482(5), 3.504(5), and 3.534(6) Å.

centers are looking for the highest electron density available, as has been seen in other organometallic complexes of $[Rh_2(O_2CCF_3)_4]$.[10,14]

To compare the coordination at the Bi site, the homometallic bismuth(II) trifluoroacetate adduct with pyrene has been synthesized. It was prepared by codeposition of $[Bi_2(O_2CCF_3)_4]$ with $C_{16}H_{10}$ at 80 °C in a sealed evacuated ampule. This reaction afforded red crystals of $[Bi_2(O_2CCF_3)_4 \cdot (C_{16}H_{10})]$ (**3**) deposited in the coldest end of the container within one week with a yield of >90%. Complex **3** is still moisture sensitive when exposed to the open atmosphere, but to a lesser degree than the unligated bismuth(II) trifluoroacetate.[11] It also shows a characteristic (though smaller than in **1**) shift in C−H stretch in the IR spectrum compared to free pyrene.

The structure of **3** consists of alternating dibismuth(II,II) tetratrifluoroacetate units and pyrene molecules that form a 1D chain polymer with a 1:1 composition of $[Bi_2(O_2CCF_3)_4]$ to $C_{16}H_{10}$ (Figure 2). The six Bi···C contacts vary in the range from 3.432(4) to 3.534(4) Å averaging 3.478 in **3**, which is close to that of 3.489 Å in **1**. These distances are all within the sum of the van der Waals radii for bismuth and carbon, $\sum r_{vdW}(Bi, C) = 4.10$ Å.[16] The Bi···$C_{centroid}$ distance of 3.18 Å is essentially the same as in the Bi−Rh complex with pyrene. The Bi−Bi bond length of 2.9538(4) Å in **3** is longer than that of 2.9462(3) Å in the unligated $[Bi_2(O_2CCF_3)_4]$ complex.[11]

DFT Calculations. Density functional theory calculations have been undertaken to evaluate the effect of one metal on the coordinating abilities of the other in the heterobimetallic $[BiRh(O_2CCF_3)_4]$ unit. The nature of metal−π-arene interactions and their energetics in the pyrene heterobimetallic complex have been compared with those in the homometallic analogues. Thus, DFT calculations have been executed for the following discrete monoadduct complexes: $[Rh_2(O_2CCF_3)_4 \cdot (\eta^2\text{-}C_{16}H_{10})]$ (**2d**), $[Bi_2(O_2CCF_3)_4 \cdot (\eta^6\text{-}C_{16}H_{10})]$ (**3d**), $[BiRh(O_2CCF_3)_4 \cdot (\eta^2\text{-}C_{16}H_{10}\text{-}Rh)]$ (**4**), and $[BiRh(O_2CCF_3)_4 \cdot (\eta^6\text{-}C_{16}H_{10}\text{-}Bi)]$ (**5**) as well as for their parent unligated dinuclear units, $[Bi_2(O_2CCF_3)_4]$ (**6**), $[Rh_2(O_2CCF_3)_4]$ (**7**), $[BiRh(O_2CCF_3)_4]$ (**8**), and pyrene (**9**) (see Supporting Information for details).

It should be mentioned here that theoretical modeling of the dimetal core compounds **6**, **7**, and **8** has been carried out previously.[6,17] However, those studies were performed at different levels of theory, which may thwart a direct comparison of all systems in this work. Therefore, all calculations have been carried out here by applying the homogeneous high-level approach in the frame of the density functional theory technique. Specifically, the parameter-free hybrid exchange−correlation functional PBE0[18] has been used. The latter was recently proven to show consistently superior results over the commonly used B3LYP functional for calculations of polynuclear metal complexes and their adducts with planar and curved polyarenes.[19] Importantly, the calculated equilibrium geometries of all systems are found to be in a good agreement with those obtained by single-crystal X-ray crystallography (Supporting Information, Tables S1, S4, S7, S13, S16, and S19).

Electronic Structures of Unligated Dimetal Complexes. Before considering the formation of pyrene adducts, some differences and similarities in the electronic structures of dimetal complexes of the general formula $[MM'(O_2CCF_3)_4]$ (M and M′ are Bi and/or Rh) should be mentioned. In the case of the dirhodium(II,II) core, atomic orbitals (AO) of only the d-type contribute to the formation of the metal−metal bond. Specifically, there are four occupied bonding molecular orbitals (MOs) and three occupied antibonding MOs (see Supporting Information for details) with only a bonding MO related to the $d_{z^2}-d_{z^2}$ metal−metal interaction, which has no corresponding occupied antibonding MO. Thus, the nature of the interaction between the two rhodium centers in $[Rh_2(O_2CCF_3)_4]$ is interpreted simplistically as a σ-type single metal−metal bond.[20] On the other hand, in the dibismuth(II,II) core complex there is only one bonding σ-type MO formed by the p_z atomic orbitals of the two metals,[21] while the corresponding antibonding orbital is one of the unoccupied MOs (LUMO+2). At the same time, the lowest unoccupied MOs in $[Bi_2(O_2CCF_3)_4]$, LUMO and LUMO+1, are bonding MOs. In $[BiRh(O_2CCF_3)_4]$, the metal−metal bond is the result of the interaction of d_{z^2}-AO of Rh with p_z-AO of Bi (Figure 3), consistent with the previous report.[6] In contrast to the electronic structure of the homometallic dirhodium complex, three d-type MOs in $[BiRh(O_2CCF_3)_4]$ are nonbonding MOs centered at the Rh site. These orbitals are the highest occupied MOs (HOMO, HOMO−1, and HOMO−2, respectively). Similarly, two unoccupied metal−metal bonding MOs in the dibismuth unit have been transformed into two nonbonding MOs centered at the Bi site of the Bi−Rh core in

(17) (a) Cotton, F. A.; Dikarev, E. V.; Feng, X. *Inorg. Chim. Acta* **1995**, *237*, 19–26. (b) Filatov, A. S.; Rogachev, A. Yu.; Petrukhina, M. A. *Crystal Growth Des.* **2006**, *6*, 1479–1484. (c) Lichtenberger, D. L.; Pollard, J. R.; Lynn, M. A.; Cotton, F. A.; Feng, X. *J. Am. Chem. Soc.* **2000**, *122*, 3182–3190.

(18) (a) Perdew, J. P.; Burke, K.; Ernzerhof, M. *Phys. Rev. Lett.* **1996**, *77*, 3865–3868. (b) Perdew, J. P.; Burke, K.; Ernzerhof, M. *Phys. Rev. Lett.* **1997**, *78*, 1396–1396. (c) Adamo, C.; Barone, V. *J. Chem. Phys.* **1999**, *110*, 6158–6170.

(19) (a) Petrukhina, M. A.; Sevryugina, Y.; Rogachev, A. Yu.; Jackson, E. A.; Scott, L. T. *Angew. Chem., Int. Ed.* **2006**, *45*, 7208–7210. (b) Zhu, B.; Ellern, A.; Sygula, A.; Sygula, R.; Angelici, R. J. *Organometallics* **2007**, *26*, 1721–1728. (c) Rogachev, A. Yu.; Sevryugina, Y.; Filatov, A. S.; Petrukhina, M. A. *Dalton Trans.* **2007**, *387*, 1–3873.

(20) Chifotides, H. T.; Dunbar, K. R. In *Multiple Bonds Between Metal Atoms*, 3rd ed.; Cotton, F. A., Murillo, C. A., Walton, R. A., Eds.; Springer Science Inc., 2005; pp 465−589.

(21) The detailed DFT results for the $[Bi_2(O_2CR)_4]$ series will be presented elsewhere.

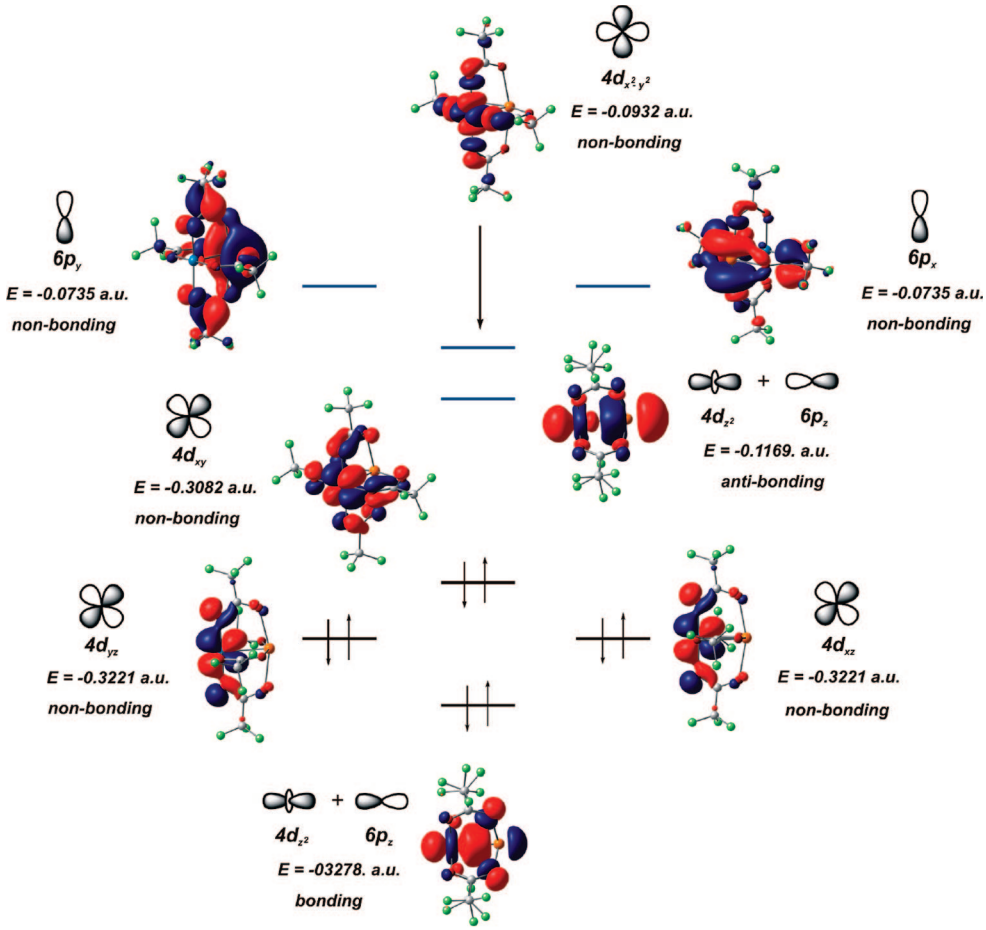

Figure 3. Metal-based frontier molecular orbitals in $[BiRh(O_2CCF_3)_4]$ (**8**) (DFT/PBE0/LANL2DZ/6-311G(d,p)).

8 (Figure 3). Moreover, some changes in MO ordering have been found in **8**, and that can affect reactivity of the Bi site in the heterobimetallic complex. In contrast to the electronic structure of $[Bi_2(O_2CCF_3)_4]$, the p-type MOs centered at the Bi site in the heterobimetallic unit are no longer LUMO and LUMO+1. The LUMO in $[BiRh(O_2CCF_3)_4]$ corresponds to the antibonding MO of the metal−metal bond, while the LUMO+1 is attributed to the nonbonding d-type MO, centered at the Rh site.

Hardness of Open Axial Sites in Dimetal Units. An analysis of the DFT frontier MOs in the unligated dimetal complexes **6**−**8** can be successfully used to estimate and to compare their chemical hardness.[22] In accord with the HSAB (hard/soft acid/base) approach,[23] an increase in the energy gap between HOMO and LUMO strongly corresponds to a gain in hardness of the molecules considered. In this regard, $[Bi_2(O_2CCF_3)_4]$ is significantly harder than $[Rh_2(O_2CCF_3)_4]$ (Table 1). Interestingly, the replacement of one Rh by Bi in $[Rh_2(O_2CCF_3)_4]$ results in a noticeable increase of chemical hardness since the Δ(HOMO−LUMO) widens from 3.58 in **7** to 5.21 eV in **8**. However, if an alternative replacement of one Bi by Rh in $[Bi_2(O_2CCF_3)_4]$ (**6**) is considered, the hardness of the resulting heterobimetallic core in **8** remains very similar to that in **6**. As a result, $[BiRh(O_2CCF_3)_4]$ is significantly harder than the homometallic dirhodium complex but only slightly softer than the dibismuth one. Since an increase of chemical hardness results in the

Table 1. Selected Calculated Geometric and Electronic Parameters of Unligated Dimetal Tetratrifluoroacetate Complexes

	$[Bi_2(O_2CCF_3)_4]$ **6**	$[Rh_2(O_2CCF_3)_4]$ **7**	$[BiRh(O_2CCF_3)_4]$ **8**
Bi−O	2.339		2.328
Rh−O		2.042	2.038
M−M	2.933	2.385	2.591
order (M−M)	0.924	0.799	0.723
q(Bi)[a]	+1.390		+1.674
q(Rh)[a]		+0.966	+0.647
Δ(HOMO−LUMO)[b]	5.65	3.58	5.21

[a] q is atomic charge. [b] The energy gap values are in eV.

(22) (a) Chemical Applications of Density Functional Theory. Baerends, E. J.; Gritsenko, O. V.; van Leuwen, R. *ACS Symp. Ser.* **1996**, *269*, 20–35. (b) Stowasser, R.; Hoffmann, R. *J. Am. Chem. Soc.* **1999**, *121*, 3414–3420.
(23) Pearson, R. G. *Chemical Hardness Applications from Molecules to Solids*; Wiley-VCH Verlag GmbH: Weinheim, 1997; p 198.
(24) (a) Barone, V.; Peralta, J. E.; Scuseria, G. E. *Nano Lett* **2005**, *5*, 1830–1833. (b) Bettinger, H. F. *Org. Lett.* **2004**, *6*, 731–734. (c) Bettinger, H. F. *J. Phys. Chem. B* **2005**, *109*, 6922–6924. (d) Ernzerhof, M.; Scuseria, G. *J. Chem. Phys.* **1999**, *110*, 5029–5036. (e) Avramov, P. V.; Kudin, K. N.; Scuseria, G. E. *Chem. Phys. Lett.* **2003**, *370*, 597–601. (f) An, W.; Gao, Y.; Bulusu, S.; Zeng, X. C. *J. Chem. Phys.* **2005**, *122*, 204109–1. (g) Johansson, M. P.; Sundholm, D.; Vaara, J. *Angew. Chem., Int. Ed.* **2004**, *43*, 2678–2681.
(25) Hay, P. J.; Wadt, W. R. *J. Chem. Phys.* **1985**, *82*, 270–283.
(26) (a) Reed, A. E.; Curtiss, L. A.; Weinhold, F. *Chem. Rev.* **1988**, *88*, 899–926. (b) Weinhold, F.; Landis, C. A. *Valency and Bonding: A Natural Bond Orbital Donor-Acceptor Perspective*; Cambridge University Press: Cambridge, 2005; p 760.
(27) Wiberg, K. *Tetrahedron* **1968**, *24*, 1083–1096.
(28) http://www.chemcraftprog.com.
(29) Granovsky, A. A. http://lcc.chem.msu.ru/gran/gamess/index.html.
(30) Schmidt, M. W.; Baldridge, K. K.; Boatz, J. A.; Elbert, S. T.; Gordon, M. S.; Jensen, J. H.; Koseki, S.; Matsunaga, N.; Nguyen, K. A.; Su, S.; Windus, T. L.; Dupuis, M.; Montgomery, J. A. *J. Comput. Chem.* **1993**, *14*, 1347–1363.

Table 2. Selected Calculated Geometric and Electronic Parameters for Pyrene and Its Monoadducts with Dimetal Tetratrifluoroacetate Complexes (see Figures S9, S11, S13, S15 for labeling)[a]

	$C_{16}H_{10}$ (L)	$[Rh_2(\eta^2\text{-L})]$ **2d**	$[Bi_2(\eta^6\text{-L})]$ **3d**	[BiRh (η^2-L-*Rh*)] **4**	[BiRh (η^6-L-*Bi*)] **5**
M−M		2.427	2.945	2.602	2.607
Rh−C(1)		2.487		2.707	
Rh−C(2)		2.489		2.710	
Bi···centroid			3.461		3.316
C(1)−C(2)	1.359	1.382	1.358	1.371	1.358
order (M−M)		0.621	0.915	0.687	0.689
order (C(1)−C(2))	1.655	1.506	1.655	1.597	1.654
q(Rh(1))		+0.927		+0.663	+0.636
q(Rh(2))		+0.871			
q(Bi(1))			+1.411	+1.592	+1.698
q(Bi(2))			+1.372		
q(C(1))	−0.180	−0.201	−0.184	−0.217	−0.186
q(C(2))	−0.180	−0.202	−0.163	−0.219	−0.157
$E_{bonding}$, kcal/mol		20.08	7.39	9.74	7.20
$E^{(2)}$, kcal/mol		46.38	8.47	22.48	10.96

[a] *q* is atomic charge, $E^{(2)}$ is estimation of donor−acceptor interactions in the frame of the second-order perturbation theory in the NBO basis. $\Delta E^{(2)}_{i\rightarrow j} = -2[\langle\sigma_i|\hat{F}|\sigma_j\rangle^2/\varepsilon_{j^*} - \varepsilon_i]$, where $\hat{F}$ is an effective orbital Hamiltonian (Fock or Kohn−Sham operator) and $\varepsilon_i = \langle\sigma_i|\hat{F}|\sigma_i\rangle$, $\varepsilon_{j^*} = \langle\sigma_{j^*}|\hat{F}|\sigma_{j^*}\rangle$ are orbital energies for the donor and acceptor natural bond orbitals, respectively.

domination of Coulombic interactions over the covalent contribution to bonding according to Pearson,[23] we should expect an overall decrease of the general donor−acceptor abilities of $[BiRh(O_2CCF_3)_4]$ relative to the well-studied homometallic $[Rh_2(O_2CCF_3)_4]$ complex.

Electronic and Geometric Structures of Dimetal Complexes with Pyrene. Since there are two metal sites of different nature in $[BiRh(O_2CCF_3)_4]$, we should consider those separately when comparing with the corresponding homometallic units (Table 2). Thus, the Rh-bound complex with pyrene, $[BiRh(O_2CCF_3)_4\cdot(\eta^2\text{-}C_{16}H_{10}\text{-}Rh)]$ (**4**), will be compared with the analogous discrete dirhodium $[Rh_2(O_2CCF_3)_4\cdot(\eta^2\text{-}C_{16}H_{10})]$ complex (**2d**). Similarly, the Bi-bound pyrene complex, $[BiRh(O_2CCF_3)_4\cdot(\eta^6\text{-}C_{16}H_{10}\text{-}Bi)]$ (**5**), will be considered along with the homometallic $[Bi_2(O_2CCF_3)_4\cdot(\eta^6\text{-}C_{16}H_{10})]$ monoadduct (**3d**).

The major difference in geometric parameters of the adducts $[Rh_2(O_2CCF_3)_4\cdot(\eta^2\text{-}C_{16}H_{10})]$ (**2d**) and $[BiRh(O_2CCF_3)_4\cdot(\eta^2\text{-}C_{16}H_{10}\text{-}Rh)]$ (**4**) (Tables 2, S16, S19, Figures S9, S11, S13, S15) is in their Rh−C distances, which are significantly longer in **4**. At the same time, the elongation of the metal−metal bond upon coordination of pyrene is greater in **2d** ($\Delta = 0.042$ Å) compared to that in **4** ($\Delta = 0.011$ Å). These facts clearly indicate that the interaction between rhodium(II) and pyrene is stronger in the homometallic complex **2d** than in **4**. This is also confirmed by the estimated bonding energy between the dimetal units and pyrene (20.08 in **2d** vs 9.74 kcal/mol in **4**). To rationalize this difference in stability, a detailed analysis of electronic structures in terms of natural bond orbitals (NBO) has been performed. It was found that the donor−acceptor interactions are greater in $[Rh_2(O_2CCF_3)_4\cdot(\eta^2\text{-}C_{16}H_{10})]$ (**2d**) compared to those in $[BiRh(O_2CCF_3)_4\cdot(\eta^2\text{-}C_{16}H_{10}\text{-}Rh)]$ (**4**), being 46.38 and 22.48 kcal/mol, respectively. The decomposition of these interactions into two components, namely, metal-to-ligand (M→L) and ligand-to-metal (L→M) contributions, has revealed the main reason for this difference. While the energies of the M→L interaction for both compounds are very close (7.97 in **2d** vs 7.52 kcal/mol in **4**), the L→M contribution is significantly larger in **2d** (38.41 kcal/mol) compared to **4** (14.96 kcal/mol). This is clearly reflected in the decrease of the C(1)−C(2) bond order of the coordinated pyrene (Table 2), which is observed in both adducts but is smaller in **4**. As a consequence, the elongation of this carbon−carbon bond is greater in the dirhodium adduct **2d**.

Scheme 2. Schematic Representation of Bonding Interactions in the Pyrene Adducts of $[Rh_2(O_2CCF_3)_4]$ (a and b) and of $[BiRh(O_2CCF_3)_4]$ (c and d)[a]

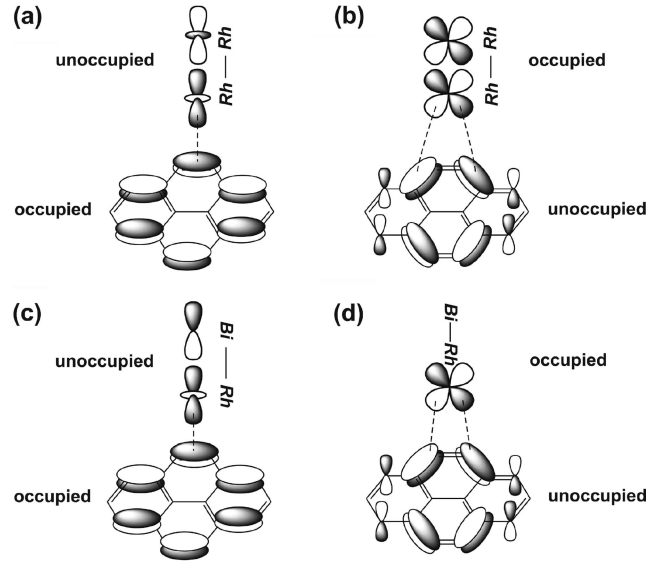

[a] (a) L→M interaction between unoccupied σ-shaped ($d_{z^2}-d_{z^2}$) antibonding MO of $[Rh_2(O_2CCF_3)_4]$ (LUMO) and HOMO of pyrene; (b) M→L interaction between one of the two degenerate π-shaped ($d_{xz}-d_{xz}$ or $d_{yz}-d_{yz}$) occupied MOs of $[Rh_2(O_2CCF_3)_4]$ (HOMO−1 or HOMO−2) and LUMO of pyrene; (c) L→M interaction between unoccupied σ-shaped ($d_{z^2}-p_z$) antibonding MO of $[BiRh(O_2CCF_3)_4]$ (LUMO) and HOMO of pyrene; (d) M→L interaction between one of the two degenerate occupied d-shaped (d_{xz} or d_{yz}) Rh-centered MOs (HOMO−1 or HOMO−2) of $[BiRh(O_2CCF_3)_4]$ and LUMO of pyrene.

The detailed analysis of the electronic structures of the adducts $[Rh_2(O_2CCF_3)_4\cdot(\eta^2\text{-}C_{16}H_{10})]$ (**2d**) and $[BiRh(O_2CCF_3)_4\cdot(\eta^2\text{-}C_{16}H_{10}\text{-}Rh)]$ (**4**) allowed us to construct the MO diagram (Figure S12) and to build the scheme of orbital interactions in these systems (Scheme 2). The characteristic feature of the interaction between the dirhodium core and an axially bound pyrene in **2d** involves the metal-to-ligand interaction that can be described as a four-electron three-orbital bond. The major contribution to bonding in **2d** results from the interaction between the lowest unoccupied MO (LUMO) of pyrene and one of the two degenerate antibonding MOs of $[Rh_2(O_2CCF_3)_4]$. The bonding description at the Rh end of the heterobimetallic Bi−Rh unit in **4** is similar. It is worth mentioning here that the detailed interaction analysis allowed us to determine the hapticity of the coordinated pyrene in **4**, which is consistent with an η^2-assignment at the Rh end.

For the next step, the theoretical modeling of $[BiRh(O_2CCF_3)_4\cdot(\eta^6\text{-}C_{16}H_{10}\text{-}Bi)]$ (**5**) has been accomplished and compared with that of $[Bi_2(O_2CCF_3)_4\cdot(\eta^6\text{-}C_{16}H_{10})]$ (**3d**). An analysis of geometric parameters of **3d** and **5** shows that the Bi···$C_{centroid}$ separation is noticeably longer in the dibismuth adduct than that in the Bi−Rh one (Table 2). At the same time, the elongation of the metal−metal bond length due to coordination of pyrene at the Bi site has been observed in both cases. In spite of the quite different metal−metal bond distances in the monoadducts (2.945 Å in **3d** and 2.607 Å in **5**), their relative elongations in comparison with the unligated dimetal units are close (0.016 and 0.012 Å, respectively). These data indicate a similar strength of interactions between the polyaromatic system

Scheme 3. Schematic Representation of Bonding L→M Interaction: (a and b) in $[Bi_2(O_2CCF_3)_4\cdot(\eta^6\text{-}C_{16}H_{10})]$ (3d); (c and d) in $[BiRh(O_2CCF_3)_4\cdot(\eta^6\text{-}C_{16}H_{10}\text{-}Bi)]$ (5)[a]

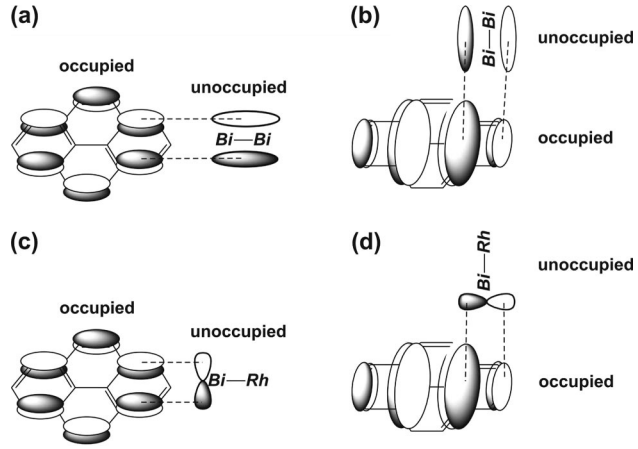

[a] (a) Interaction between the first of the two degenerate unoccupied π-shaped (p_x-p_x) MOs of $[Bi_2(O_2CCF_3)_4]$ (LUMO) and HOMO of pyrene; (b) interaction between the second of the two degenerate unoccupied π-shaped (p_y-p_y) MOs and HOMO−1 of pyrene; (c) interaction between the first degenerate p-shaped unoccupied Bi-centered MO (LUMO+3) of $[BiRh(O_2CCF_3)_4]$ and HOMO of pyrene; (d) interaction between the second degenerate unoccupied p-shaped Bi-centered MOs of $[BiRh(O_2CCF_3)_4]$ and HOMO−1 of pyrene.

and the dimetal core in both adducts, which is in good agreement with their estimated bonding energies (7.39 in **3d** and 7.20 kcal/mol in **5**).

In this regard, it is informative to compare the nature of interaction between the Bi site of the dimetal units and pyrene in $[Bi_2(O_2CCF_3)_4\cdot(\eta^6\text{-}C_{16}H_{10})]$ (**3d**) and $[BiRh(O_2CCF_3)_4\cdot(\eta^6\text{-}C_{16}H_{10}\text{-}Bi)]$ (**5**). A detailed analysis of their electronic structures allowed us to estimate the energy of donor−acceptor interactions (8.47 in **3d** vs 10.96 kcal/mol in **5**) in the frame of the NBO technique. In spite of quite close values, the nature of these interactions is different. The M→L and L→M contributions are similar in **3d** (4.03 and 4.44 kcal/mol, respectively) but distinctly different in the heterobimetallic adduct **5** (1.63 and 9.33 kcal/mol). The simplified diagram of the L→M contribution to donor−acceptor interactions for both adducts is presented in Scheme 3.

In this work, the theoretical approach successfully used for modeling the Rh(II)−arene complexes has been expanded to describe Bi(II) adducts. The MO diagram shows that both orthogonal π-shaped bonding molecular orbitals centered at the dibismuth core are involved in the interaction with two orthogonal MOs (HOMO and HOMO−1) of pyrene. Since these MOs belong only to the delocalized benzene rings (Scheme 3, Figure S8, Scheme S1), all six carbon atoms of those rings participate in bonding with the Bi(II) center, and the hapticity of such interaction is η^6. This assignment is confirmed by analysis of donor−acceptor interactions in terms of the NBO approach, indicating that each carbon atom of the coordinated benzene rings provides an approximately equal contribution to the L→M interaction. Moreover, the specificity of the Bi−pyrene coordination can be explained from this point of view. Two π-shaped unoccupied bonding MOs centered at the dibismuth core should interact with two degenerate orthogonal (or really close on the energy scale) π-shaped occupied MOs of an axially bound aromatic ligand. In pyrene such orbitals are localized only at the benzene ring considered, and this should determine the site-specific coordination of Bi(II) to $C_{16}H_{10}$.

Table 3. Crystallographic Data for $[BiRh(O_2CCF_3)_4\cdot(C_{16}H_{10})]_\infty$ (1) and $[Bi_2(O_2CCF_3)_4\cdot(C_{16}H_{10})]_\infty$ (3)

	1	3
formula	$BiRhO_8C_{24}F_{12}H_{10}$	$Bi_2O_8C_{24}F_{12}H_{10}$
fw	966.21	1072.28
cryst syst	triclinic	triclinic
space group	$P\bar{1}$	$P\bar{1}$
a (Å)	8.5229(4)	8.2529(10)
b (Å)	12.8739(6)	9.3214(11)
c (Å)	13.1035(6)	9.8706(12)
α (deg)	81.988(1)	91.121(2)
β (deg)	85.192(1)	110.040(2)
γ (deg)	71.631(1)	100.932(2)
V (Å^3)	1349.96(11)	697.46(15)
Z	2	1
ρ_{calcd} (g·cm^{-3})	2.377	2.553
μ (mm^{-1})	7.252	12.726
radiation (λ, Å)	Mo Kα (0.71073)	Mo Kα (0.71073)
transm factors	0.2863−0.5946	0.2512−0.4695
temp (K)	90(2)	90(2)
data/restr/params	415/0/5791	237/18/3106
R1,[a] wR2[b]		
$I > 2\sigma(I)$	0.0234, 0.0223	0.0265, 0.0668
all data	0.0578, 0.0572	0.0290, 0.0681
quality-of-fit[c]	1.082	1.085

[a] $R1 = \sum||F_o| - |F_c||/\sum|F_o|$. [b] $wR2 = [\sum[w(F_o^2 - F_c^2)^2]/\sum[w(F_o^2)^2]]^{1/2}$. [c] Quality-of-fit $= [w(F_o^2 - F_c^2)^2]/(N_{obs} - N_{params})]^{1/2}$, based on all data.

Regarding the nature of interactions between a metal center and polyaromatic molecules such as pyrene, orbital control should play an important role and make a great contribution to bonding between the interacting units. However, the detailed analysis of the electronic structures of all pyrene adducts shows that the donor−acceptor interactions have a noticeable contribution to bonding due to electron transfer only in the case of the rhodium-bound complexes $[Rh_2(O_2CCF_3)_4\cdot(\eta^2\text{-}C_{16}H_{10})]$ (**2d**) and $[BiRh(O_2CCF_3)_4\cdot(\eta^2\text{-}C_{16}H_{10}\text{-}Rh)]$ (**4**). At the same time, a strong influence of metal charge on bonding energy has been found. The replacement of one bismuth ion in $[Bi_2(O_2CCF_3)_4]$ by rhodium leads to a charge increase at the Bi site from +1.39 in the former to +1.67 in $[BiRh(O_2CCF_3)_4]$. This change is expected to show up as a gain of bonding energy in the Bi-bound adduct, $[BiRh(O_2CCF_3)_4(\eta^6\text{-}C_{16}H_{10}\text{-}Bi)]$ (**5**). Additionally, the coordination of pyrene by bismuth(II) leads to polarization of the former. The resulting negative charges at the coordinated benzene ring of pyrene in **5** become noticeably greater than those in an uncoordinated one (see Supporting Information). Thus, the overall interactions between the Bi site and pyrene can be described as Coulombic interactions between the highly charged metal center and an induced dipole of pyrene under strong orbital control.

At the same time, the charge at the rhodium center in $[BiRh(O_2CCF_3)_4]$ (**8**) is lower than that in dirhodium complex **7** (+0.65 vs +0.97, respectively). This should ultimately affect the bonding energy between the dimetal core and pyrene, which is greater in the homometallic $[Rh_2(O_2CCF_3)_4(\eta^2\text{-}C_{16}H_{10})]$ adduct (**2d**) than in $[BiRh(O_2CCF_3)_4(\eta^2\text{-}C_{16}H_{10}\text{-}Rh)]$ (**4**). The difference in stability between **2d** and **4** is also induced by different contributions of donor−acceptor interactions (Table 2), which are significantly greater for the former. Thus, the covalent contribution to bonding energy in **4** is lower than that in **2d**, but it is noticeably higher than that in the Bi-bound adducts **3d** and **5**. So the nature of bonding between the Rh-site and pyrene in **4** can be successfully described as a combination of donor−acceptor and Coulombic interactions between the positively charged metal center and an induced dipole moment of an axial arene ligand. Moreover, this interaction has a strong orbital control defining the site-

specificity of coordination. A comparison of the nature of interactions between the Rh and Bi sites of the $[BiRh(O_2CCF_3)_4]$ unit and pyrene indicates that a decrease of Coulombic contribution in **4** is compensated by the corresponding increase of the donor−acceptor one. As a result, the overall bonding energies of the two isomers $[BiRh(O_2CCF_3)_4(\eta^2\text{-}C_{16}H_{10}\text{-}Rh)]$ and $[BiRh(O_2CCF_3)_4(\eta^6\text{-}C_{16}H_{10}\text{-}Bi)]$ are similar, while the nature of the bonding is different at the two opposite ends of the heterobimetallic core.

"Intelligent" Assembly from the Gas Phase Deposition Reaction. Complex $[BiRh(O_2CCF_3)_4\cdot(C_{16}H_{10})]$ (**1**) represents a unique example of site-controlled arene coordination at the different metal sites of a heterobimetallic unit. Specifically, it features η^6-coordination of pyrene at the Bi end and η^2-coordination at the Rh end, which have been confirmed both crystallographically and computationally. In addition, a remarkable feature of the title complex is the alternation of the $\eta^2{:}\eta^2$ and $\eta^6{:}\eta^6$ bridging modes of pyrene in the 1D polymeric solid state structure.

The assembly of the 1D chain of **1** can be considered a step-by-step growth from discrete building units existing or formed in the vapor phase. It is noteworthy that in all our previous solventless reactions utilizing dimetal units and bidentate ligands this process could simply be explained by the formation of one type of building block in the gas phase, mostly monoadducts, that form extended chains upon deposition. In those cases, each subsequent step of the chain formation was a trivial repetition of the previous one and required assembling the same units in a similar fashion. In other words, the chain growth from the gas phase at elevated temperatures was found to be neither selective nor discriminatory. If such an assembly process was applied to the Bi−Rh system with pyrene, it would result in the $\eta^2{:}\eta^6$ isomer of $[BiRh(O_2CCF_3)_4\cdot(C_{16}H_{10})]_\infty$. In contrast, the formation of **1** is different and more complicated. It not only requires the presence of at least two different species in the vapor phase but also needs an "intelligent" character for the chain assembly. In order to form **1**, possible combinations of the two building units may include (i) [Bi−Rh] and $(C_{16}H_{10})$, (ii) $[Bi{-}Rh(\eta^2\text{-}C_{16}H_{10}\text{-}Rh)]$ and $[Bi{-}Rh(\eta^6\text{-}C_{16}H_{10}\text{-}Bi)]$, or (iii) $[(\eta^6\text{-}C_{16}H_{10}\text{-}Bi)Bi{-}Rh(\eta^2\text{-}C_{16}H_{10}\text{-}Rh)]$ and [Bi−Rh]. However, regardless of the nature of these species, every next step in the assembly process differs from the previous one. It requires an alternation of two building units each time and, in some cases, a specific orientation of a unit in order to propagate the chain.

We do not have means to prove which species exist in the gas phase. However, the facts that the yield of **1** is nearly quantitative and that the deposition of the bis-pyrene adduct $[(\eta^6\text{-}C_{16}H_{10}\text{-}Bi)Bi{-}Rh(\eta^2\text{-}C_{16}H_{10}\text{-}Rh)]$ or the unligated [Bi−Rh] complex has never been seen in this reaction at variable conditions allow us to speculate that the two monoadducts, case ii, are the most probable building units. The latter should have similar volatilities, unlike the species in the cases i and iii. DFT calculations of these isomeric complexes with pyrene, namely, $[Bi{-}Rh(\eta^2\text{-}C_{16}H_{10}\text{-}Rh)]$ and $[Bi{-}Rh(\eta^6\text{-}C_{16}H_{10}\text{-}Bi)]$, have shown that the Rh derivative is only slightly more stable ($\Delta E = 2.54$ kcal/mol). This difference may become negligible at the elevated temperatures used in synthesis, resulting in an almost equal distribution of the two complex units in the vapor phase and thus allowing their even condensation for the growth of **1**. Their 1:1 alternation would be sufficient to form the polymeric structure **1** but requires a specific orientation of building units for the chain propagation. This may be explained by the fact that the coordinated pyrene in both monoadducts is activated in a specific way. When an arene has Rh bound to one end, it is able to coordinate Rh only at the opposite pyrene end in an η^2-site specific mode. In the case of the Bi-bound adduct, the activation of pyrene leads to the Bi binding only at the opposite ring of $C_{16}H_{10}$. The selection of the proper building unit from the gas phase would result in the alternation of the $\eta^2{:}\eta^2$ and $\eta^6{:}\eta^6$ bridging modes of pyrene and thus dictates the "intelligent" stepwise assembly of the extended solid state structure of **1**.

Experimental Section

General Procedures. All of the manipulations were carried out in a dry, oxygen-free, dinitrogen atmosphere by employing standard glovebox and Schlenk techniques. All chemicals, unless otherwise described, were purchased from Aldrich and used as received. $[Bi_2(O_2CCF_3)_4]$ and $[BiRh(O_2CCF_3)_4]$ were synthesized using the procedures that we reported previously.[6,11] The attenuated total reflection (ATR) and solution IR spectra were recorded on a Perkin-Elmer Spectrum 100 FT-IR spectrometer. NMR spectra were obtained using a Bruker Avance 400 spectrometer at 400 MHz for ^{1}H and at 376.47 MHz for ^{19}F. Chemical shifts (δ) are reported in ppm relative to residual solvent peaks for ^{1}H and to $CFCl_3$ for ^{19}F. Elemental analyses were performed by Maxima Laboratories Inc., Ontario, Canada.

Synthesis of $[BiRh(O_2CCF_3)_4\cdot(C_{16}H_{10})]$ (1). A mixture of $BiRh(O_2CCF_3)_4$ (0.034 g, 0.050 mmol) and pyrene (0.040 g, 0.20 mmol) was sealed in an evacuated glass ampule. It was kept at 100 °C (hot zone, $\Delta T = 6$ °C) for a week to allow red crystals of **1** to be deposited in the cold zone. Yield: >90%. Anal. Calcd: C, 29.83; H, 1.04; O, 13.25; F, 23.60; Bi, 21.63; Rh, 10.65. Found: C, 30.20; H, 1.10; O, 12.85; F, 23.02; Bi, 22.02; Rh, 10.07. ^{1}H NMR (CD_2Cl_2, 22 °C): δ 8.03 (t, CH, $J = 7.47$ Hz), 8.11 (s, CH), 8.21 (d, CH, $J = 7.61$ Hz). ^{19}F NMR ($CDCl_3$, 22 °C): δ −72.83 (s, CF_3). ATR-IR (cm^{-1}): 3055w(*C−H*), 1653s, 1610sh (ν_{asym}(*COO*)), 1591m-(*C═C*), 1452m(ν_{sym}(*COO*)), 1435m(*C═C*), 1213s, 1188s, 1155s, 1098s, 975m, 858s, 847s, 788s, 733s, 721s, 709s. IR (CCl_4, cm^{-1}): 3054w(*C−H*), 1654s (ν_{asym}(*COO*)), 1590w(*C═C*), 1453w-(ν_{sym}(*COO*)), 1435w(*C═C*), 1218s, 1192s, 1171s, 859m, 847m.

Synthesis of $[Bi_2(O_2CCF_3)_4\cdot(C_{16}H_{10})]$ (3). A mixture of $Bi_2(O_2C-CF_3)_4$ (0.044 g, 0.050 mmol) and pyrene $C_{16}H_{10}$ (0.040 g, 0.20 mmol) was sealed in an evacuated glass ampule. The ampule was kept at 80 °C (hot zone, $\Delta T = 6$ °C) for one week to allow red crystals of **3** to be deposited in the cold zone. Yield: >90%. Anal. Calcd: C, 26.88; H, 0.94; O, 11.94; F, 21.26; Bi, 38.98. Found: C, 26.67; H, 1.09; O, 11.19; F, 21.24; Bi, 39.33. ^{1}H NMR ($CDCl_3$, 22 °C): δ 7.97 (t, CH, $J = 7.47$ Hz), 8.03 (s, CH), 8.17 (d, CH, $J = 7.61$ Hz). ^{19}F NMR ($CDCl_3$, 22 °C): δ −73.53 (s, CF_3). ATR-IR (cm^{-1}): 3050w(*C−H*), 1639s(ν_{asym}(*COO*)), 1600m(*C═C*), 1441m(ν_{sym}(*COO*)), 1435m(*C═C*), 1210s, 1180s, 1158s, 1138s, 973m, 844s, 792s, 755m, 723s, 709s. IR (CCl_4, cm^{-1}): 3048w-(*C−H*), 1667sh, 1640m(ν_{asym}(*COO*)), 1600w(*C═C*), 1444w(ν_{sym}-(*COO*)), 1435w(*C═C*), 1227m, 1187m.

X-ray Crystallographic Procedures. The X-ray data sets were collected for **1** and **3** at 90(2) K (Bruker KRYOFLEX) on a Bruker SMART APEX CCD-based X-ray diffractometer system equipped with a Mo target X-ray tube ($\lambda = 0.71073$ Å) operated at 1800 W power. The frames were integrated with the Bruker SAINT software package, and the data were corrected for absorption using the SADABS program. The structures were solved and refined using the Bruker SHELXTL software. All non-hydrogen atoms were refined anisotropically except the fluorine atoms of some CF_3 groups, which appeared to be disordered over three rotational orientations. Hydrogen atoms were included at idealized positions for structure factor calculations (**1**) or found in difference Fourier maps and refined independently (**3**). Relevant crystallographic data for **1** and **3** are summarized in Table 3.

DFT Calculation Details. Geometry Optimization. Full geometry optimization for all compounds was performed at the density

functional theory level using the hybrid Perdew−Burke−Ernzerhof parameter-free exchange−correlation functional (PBE0),[18] which was proposed to better describe coordination compounds of heavy metals with weak bonding. Also, this functional was successfully applied for modeling of structures and properties of curved polyaromatic systems such as nanotubes and their complexes with metal ions.[19,24] The Hay and Wadt effective core potentials (ECP)[25] and the LANL2DZ basis sets were used for Rh and Bi atoms. The standard 6-31G(d) basis sets were applied for all nonmetallic atoms. The D_{2h} point group symmetry was used for modeling of pyrene ($C_{16}H_{10}$). The C_4 point group symmetry constraints were imposed for modeling of $[Rh_2(O_2CCF_3)_4]$, $[Bi_2(O_2CCF_3)_4]$, and $[BiRh(O_2CCF_3)_4]$. Calculations of structures and properties of all adducts were performed without any symmetry constraints (C_1 point group of symmetry). The gradient norm for the geometry optimization was taken to be 10^{-4}. The true minima on potential energy surfaces were controlled by calculating the Hessian matrix and, as a consequence, harmonic frequencies. The lack of imaginary frequencies has indicated that the true minimum was achieved.

Single-Point Calculations. When optimizations were accomplished, single-point calculations were performed using the same ECP and the same basis set for Rh atoms and the extended 6-311G(d,p) basis sets for all remaining atoms. The natural bond orbital (NBO)[26] analysis based on single-point calculations was used for a detailed description of the electronic structures of compounds. Bond orders quoted in the text are those from the Wiberg formulation (so-called Wiberg bond indexes)[27] incorporated in the NBO analysis. Optimized geometry configurations and molecular orbitals (0.035 au isosurface) are visualized with the help of the ChemCraft program package.[28] All calculations were carried out in the frame of the PC GAMESS version[29] of the GAMESS-US program package[30] for quantum chemistry modeling.

Acknowledgment. We thank the donors of the American Chemical Society Petroleum Research Fund, 44770-AC3 (E.V.D.) and 42910-AC3 (M.A.P.), and the National Science Foundation, CHE-0718900 (E.V.D.) and CHE-CAREER-0546945 (M.A.P.), for support of this work.

Supporting Information Available: Computation details and tabular materials, as well as two CIF files providing crystallographic data for compounds **1** and **3**. This material is available free of charge via the Internet at http://pubs.acs.org.

OM8001763